https://doi.org/10.5194/mr-2024-4
Preprint. Discussion started: 21 February 2024

MAGNETIC RESONANCE
Discussions

Dynamic averaging of anisotropic interactions and its dependence on motional time scales in MAS solid-state NMR

Kathrin Aebischer[1], Lea Marie Becker[2], Paul Schanda[2], and Matthias Ernst[1]

[1]Department of Chemistry and Applied Biosciences, ETH Zürich, Vladimir-Prelog-Weg 2, 8093 Zürich, Switzerland
[2]Institute of Science and Technology Austria (ISTA), Am Campus 1, 3400 Klosterneuburg, Austria.

Correspondence: Matthias Ernst (maer@ethz.ch)

Abstract.

Dynamic processes in molecules can occur on a large range of time scales, and it is important to understand which time scales of motion contribute to different parameters used in dynamics measurements. For spin relaxation, this can easily be understood from the sampling of the spectral-density function by different relaxation-rate constants. In addition to data from relaxation measurements, determining dynamically-averaged anisotropic interactions in magic-angle spinning (MAS) solid-state NMR allows better quantification of the amplitude of molecular motion. For partially averaged anisotropic interactions, the relevant time scales of motion are not so clearly defined and whether the averaging depends on the experimental methods (e.g., pulse sequences) or conditions (e.g., MAS frequency, magnitude of anisotropic interaction, rf-field amplitudes) is not fully understood. To investigate these questions, we performed numerical simulations of dynamic systems based on the stochastic Liouville equation using several experiments for recoupling the dipolar-coupling, CSA or quadrupolar coupling. The transition between slow motion, where parameters characterizing the anisotropic interaction are not averaged, and fast motion, where the tensors are averaged leading to a scaled anisotropic quantity, occurs over a window of motional rate constants that depends mainly on the strength of the interaction. This transition region can span two orders of magnitude in exchange-rate constants (typically in the μs range) but depends only marginally on the employed recoupling scheme or sample spinning frequency. Residual couplings in off-magic-angle experiments, however, average over longer time scales of motion. While in principle one may gain information on the time scales of motion from the transition area, extracting such information is hampered by low signal-to-noise ratio in experimental spectra due to fast relaxation that occurs in the same region.

1 Introduction

Nuclear magnetic resonance (NMR) spectroscopy is unique in its ability to probe molecular motions with a resolution of individual atoms or bonds, and allows quantification of the amplitudes and time scales of the motional processes. In magic-angle spinning (MAS) solid-state NMR, two types of approaches are widely used to probe dynamic processes. One class of experi-

https://doi.org/10.5194/mr-2024-4
Preprint. Discussion started: 21 February 2024

ments measures nuclear spin-relaxation rate constants, which are sensitive to the local fluctuating magnetic fields generated by anisotropic interactions, i.e., the dipolar couplings to spatially close spins, the chemical-shift anisotropy (CSA) of the nucleus, or (for spins with $I > 1/2$) the quadrupolar coupling (Lewandowski, 2013; Lamley and Lewandowski, 2016; Krushelnitsky et al., 2013; Schanda and Ernst, 2016). Relaxation rate constants vary in their sensitivities to different time scales of motion by sampling the spectral-density function at different frequencies. For example, relaxation of a $^{15}N_z$ spin state (T_1 relaxation) due to the ^1H-^{15}N dipolar coupling is fastest if the motion occurs on a nanosecond time scale, while relaxation of $^{15}N_{x,y}$ coherence in the presence of a spin-lock radio-frequency field ($T_{1\rho}$ relaxation) is fastest when it takes place on a µs time scale (Schanda and Ernst, 2016). Spin relaxation measurements can, therefore, be used to extract the amplitudes and time scales of the motion. However, disentangling amplitudes and time scales is difficult and the solution may be ambiguous if multiple motions on different time scales are present (Zumpfe and Smith, 2021). For instance, using only ^{15}N T_1 and $T_{1\rho}$ relaxation times in proteins leads to a systematic underestimation of the amplitude of motion (Haller and Schanda, 2013; Lamley et al., 2015).

The second type of approach measures how anisotropic interactions, e.g., dipolar couplings, chemical-shift tensors or quadrupolar couplings, are averaged by motion (Brüschweiler, 1998; Hou et al., 2012; Yan et al., 2013; Schanda and Ernst, 2016; Watt and Rienstra, 2014). The orientation dependence of these interactions leads to motional averaging, resulting in an interaction that is the average over all the sampled conformational states. As these second-rank tensors are traceless, the time-averaged interaction strength becomes zero in the limiting case where all orientations in space are sampled with equal probability (isotropic motion). Thus, in the presence of overall tumbling, i.e., in isotropic solution, anisotropic interactions are averaged to zero, and provide no direct information about dynamics. The interactions are, however, the source of relaxation by generating fluctuating local fields. Restricted motion without overall tumbling results in a reduced magnitude of the tensor. Depending on the symmetry of the motional process, the symmetry of the tensor can change under dynamic averaging. For motional processes with at least three-fold symmetry, the tensor is characterized by a single parameter, the tensor anisotropy, δ. For a dipolar coupling the averaged and thus reduced anisotropy, $\delta_{\mathrm{IS}}^{\mathrm{red}}$, and the ratio of this value over the tensor anisotropy for the rigid-limit case, $\delta_{\mathrm{IS}}^{\mathrm{rigid}}$, report on the amplitude of the motion. It is often expressed as the dipolar order parameter, $S_{\mathrm{IS}} = \delta_{\mathrm{IS}}^{\mathrm{red}}/\delta_{\mathrm{IS}}^{\mathrm{rigid}}$. The rigid-limit tensor parameters are well known for a one-bond dipolar coupling, where the anisotropy $\delta_{\mathrm{IS}}^{\mathrm{rigid}}$ only depends on the distance between the spins and their gyromagnetic ratios, and the tensor asymmetry η is zero. For chemical-shift anisotropy and quadrupolar couplings, obtaining the rigid-limit value is only possible from quantum-chemical calculations or by freezing out the averaging process. The first approach can be very demanding for larger molecules while the latter one is experimentally complex due to the loss of resolution in low-temperature MAS NMR experiments (Concistrè et al., 2014). In the general case, dynamically averaged anisotropic interactions can become asymmetric ($\eta \neq 0$), even if the rigid-limit tensors are axially symmetric. One can exploit this feature to reveal motions with no (or low) symmetry, such as aromatic ring flips or side-chain motions in proteins from determining not only the residual anisotropy $\delta_{\mathrm{IS}}^{\mathrm{red}}$ but also the residual asymmetry parameter $\eta_{\mathrm{IS}}^{\mathrm{red}}$ (Hong, 2007; Gauto et al., 2019; Schanda et al., 2011).

https://doi.org/10.5194/mr-2024-4
Preprint. Discussion started: 21 February 2024

The efficiency of the averaging process depends on the time scale of the underlying motion: in the limiting case of very slow motion, the rigid-limit interaction strength is observed, while in the opposite extreme of very fast motion the observed interaction strength reflects the population-weighted average over the sampled conformations. The exact time scale of the transition region between these two regimes and whether it depends on the way the interaction is measured, is not entirely clear. It is often stated that the averaging is effective over all motions with a time scale shorter than the inverse of the interaction strength, e.g., tens of µs for a typical one-bond ^{1}H-^{13}C dipolar coupling (Chevelkov et al., 2023). How broad the transition region between the "fast" regime (averaged interaction strength) and "slow" regime (rigid-limit interaction) is, is not fully understood. This is, however, an important question since it defines which time scales are characterized by the measured order parameter and has several important implications. Firstly, this knowledge allows the assignment of a lower limit on the time scale of the underlying motional averaging processes observed in experiments and is crucial when measurements of dynamically averaged anisotropic interactions are used in combination with relaxation data. Such a combination is invaluable, since the order parameter, S, obtained from the averaging of anisotropic interactions, greatly improves the fit of motional time scales from relaxation data. For example, in the commonly employed detectors approach (Smith et al., 2018; Zumpfe and Smith, 2021) used for fitting relaxation data, dynamics is described by the amplitudes of motion in different time windows. Different relaxation rate constants exhibit varying sensitivities across distinct windows. The total motional amplitude, composed of the amplitudes within each of these time windows, is conveniently limited to the one derived from averaged anisotropic interactions (mostly from dipolar couplings, $1 - S^2_{\mathrm{IS}}$). However, for this approach to be rigorous, one needs to make sure that all time windows used in the detectors are indeed "seen" by the averaged anisotropic interaction.

Furthermore, understanding the time scales over which motional averaging occurs can provide information on the time scale of the underlying motion from different experimental measurements of anisotropic interactions. For example, if the same parameter, such as the dipolar-coupling derived order parameter, can be measured by different experiments that involve averaging over different time windows, any disparities in the observed order parameter would indicate motion on time scales detected by one experiment but not the other. If different approaches were to average different time scales, measuring the same tensor with a variety of methods may provide information on the time scale of motion. In MAS solid-state NMR experiments, measuring anisotropic interactions usually requires the use of a recoupling sequence since second-rank interactions are averaged out to first order by the MAS. Over the years, many different experiments have been reported for measuring dipolar couplings, including cross-polarization (CP) variants (Hong et al., 2002; Chevelkov et al., 2009; Lorieau and McDermott, 2006; Chevelkov et al., 2023), DIPSHIFT (Munowitz et al., 1981; Jain et al., 2019b), REDOR (Gullion and Schaefer, 1989; Gullion, 1998; Schanda et al., 2010; Jain et al., 2019a) and R sequences (Zhao et al., 2001; Levitt, 2007; Hou et al., 2011). Moreover, quadrupolar couplings can be measured under MAS to gain insight into dynamics (Shi and Rienstra, 2016; Akbey, 2022, 2023). In these recoupling experiments, the observed oscillation frequency that provides information on the tensor characterizing the anisotropic interaction depends on the type of experiment used, and on the exact parameters (e.g., radio-frequency (rf) field strengths and timing) of a given technique. Whether the dynamic averaging also depends on these experimental details has not been analysed

https://doi.org/10.5194/mr-2024-4
Preprint. Discussion started: 21 February 2024

systematically.

In this work, we use numerical simulations based on the stochastic Liouville equation (Kubo, 1963; Vega and Fiat, 1975; Moro and Freed, 1980; Abergel and Palmer, 2003) to investigate the averaging of anisotropic interactions by dynamics over a large range of time scales. We study how the dipolar coupling, chemical-shift anisotropy and quadrupolar coupling are averaged by motion under different experimental conditions. By examining the dependence of the observed tensor parameters on the experimental scheme employed, the size of the rigid-limit tensor and the MAS frequency, we provide a quantitative understanding of motional averaging of these parameters. This allows us to characterize which parameters determine the range of motional processes that are seen by the partially averaged anisotropic interactions.

2 Methods

Numerical simulations of dipolar and CSA recoupling as well as quadrupolar spectra under MAS were performed using the GAMMA spin simulation environment (Smith et al., 1994). Restricted molecular motion was modeled by a three-site jump process corresponding to a rotation around a C_3 symmetry axis (see Fig. 1a). The discrete states used in the jump model only differ in the orientation of the tensors characterizing the anisotropic interactions of interest (dipolar coupling, CSA, quadrupolar coupling). The simulations are based on the stochastic Liouville equation (Kubo, 1963; Vega and Fiat, 1975; Moro and Freed, 1980; Abergel and Palmer, 2003) and are performed in the composite Liouville space of the three states (see Fig. 1b for a schematic depiction of the resulting Liouvillian). The dynamic process is included in the simulations through the addition of an exchange super operator. Exchange-rate constants between $1\ \mathrm{s}^{-1}$ and $5 \cdot 10^{11}\ \mathrm{s}^{-1}$ were simulated (values of 1, 2 and 5 per decade) and a symmetric exchange process and, thus, equal populations of all states assumed (skewed populations would reduce the symmetry of the jump process). The correlation time of this three-site jump process is related to the exchange-rate constant as $\tau_{\mathrm{ex}} = \frac{1}{3k_{\mathrm{ex}}}$. To simplify the data evaluation, only axially-symmetric tensors were considered, i.e., tensors for which the asymmetry parameter $\eta = 0$. Fast exchange leads to the alignment of the scaled anisotropic interaction tensor along the symmetry axis of the three-site jump process. Therefore, the tensor has zero asymmetry both in the static and in the dynamic case and the scaling can be characterized by a single order parameter.

For dipolar recoupling, heteronuclear I-S two-spin spin-1/2 systems with different dipolar-coupling strengths, characterized by the anisotropy of the dipolar coupling tensor δ_{IS}, were simulated. The anistropy is defined as $\delta_{\mathrm{IS}} = -\frac{2\mu_0\hbar}{4\pi}\frac{\gamma_{\mathrm{I}}\gamma_{\mathrm{S}}}{4\pi {r_{\mathrm{IS}}}^3}$, where $\gamma_{\mathrm{I/S}}$ corresponds to the gyromagnetic ratios of spins I and S respectively, r_{IS} to the internuclear distance, μ_0 is the permeability of vacuum and $\hbar$ the reduced Planck constant. In these simulations, isotropic and anisotropic chemical shifts, as well as J couplings were neglected. In the case of the CSA recoupling simulations, a one-spin spin-1/2 system was simulated with changing CSA, characterized by the tensor anisotropy δ_{CSA}, while the isotropic chemical shift and the tensor asymmetry η were set to zero. Spectra of deuterium (^{2}H, spin-1 nucleus) were simulated to study the effect of dynamics on quadrupolar nuclei (one-spin system). First- and second-order quadrupolar interactions were taken into account and simulations performed at a static mag-

https://doi.org/10.5194/mr-2024-4
Preprint. Discussion started: 21 February 2024

netic field of 18.7 T corresponding to a proton Larmor frequency of 800 MHz. Based on literature values (Shi and Rienstra, 2016; Akbey, 2023), a quadrupolar coupling of $C_{\mathrm{qcc}} = 160$ kHz corresponding to an anisotropy of the quadrupolar coupling tensor of $\delta_{\mathrm{Q}}/(2\pi) = C_{\mathrm{qcc}}/(2I(2I-1)) = 80$ kHz was used. The quadrupolar tensor was assumed to be axially symmetric. All simulations were performed in the usual Zeeman rotating frame. Simultaneous averaging over all three powder angles was achieved according to the ZCW scheme (Cheng et al., 1973) and 538 to 10000 crystallite orientations used. For simulations of quadrupoles, 10000 crystallites were required to ensure sufficient γ-angle averaging and avoid phase errors in the side-band spectra. Simulation parameters are summarized in Table S1 in the SI.

In the limit of fast exchange, restricted molecular motion will lead to partial averaging of anisotropic interactions and, thus, to a scaling of the observed interaction. The scaling factor, often referred to as the order parameter S depends on the amplitude of the underlying motion. For the three-site exchange process considered here, it is determined by the opening angle θ (see Fig. 1a) and given by $P_2(\cos\theta)$, where P_2 is the second-order Legendre polynomial. In order to determine motional time scales that result in a scaling of the anisotropic interaction of interest, apparent tensor anisotropies δ^{fit} were obtained by χ^2 fitting. For this purpose, reference simulations without exchange were performed for a grid of interaction strengths (δ_{IS} for dipolar recoupling, δ_{CSA} for CSA recoupling, δ_{Q} for quadrupolar simulations). All other parameters of this reference set were the same as for the simulations with exchange and the simulated time-domain data used for the fit. For quadrupolar and off-magic-angle spinning simulations, rapid signal decay was observed for some motional time scales. Therefore, exponential line broadening was applied to the reference simulations in the time domain as $\exp(-\pi\lambda_{\mathrm{lb}}t)$ prior to χ^2 fitting and a two-dimensional grid of δ and λ_{lb} used. For pulse-sequence based dipolar and CSA recoupling, including λ_{lb} in the fitting procedure only had negligible impact on the resulting δ^{fit} and was, therefore, omitted (see Fig. S4 in the SI for a comparison of the fitting routines). Data processing was done using the Python packages numpy and matplotlib (Harris et al., 2020; Hunter, 2007) (for CSA recoupling) and Matlab (The MathWorks Inc., Natick, MA, U.S.A., all other simulations).

3 Results and Discussion

3.1 Dipolar Recoupling

Magic-angle spinning averages all second-rank anisotropic interactions and removes the heteronuclear dipolar couplings. Experimentally, there are two possible ways to reintroduce them in order to allow measurements of the dipolar order parameters. One can either use pulse sequences that interfere with the averaging by MAS, so-called dipolar recoupling sequences (Nielsen et al., 2012) or one can change the angle of the sample rotation axis slightly off the magic angle (Martin et al., 2015). The first approach can be implemented using standard MAS probes while the second requires either specialized hardware to change the spinning angle during the experiment or a permanent detuning of the spinning angle leading to line broadening in all spectral dimensions. We will discuss the effects of dynamics in both implementations.

https://doi.org/10.5194/mr-2024-4
Preprint. Discussion started: 21 February 2024

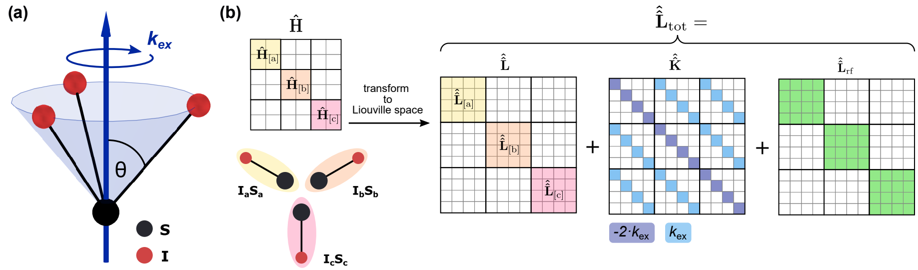

Figure 1. a) Schematic representation of the exchange model used to mimic restricted molecular motion. The dynamic process was modeled using a three-site jump model corresponding to a rotation around a C_3 symmetry axis. The time scale of this motion is characterized by the exchange-rate constant k_{ex} and the only difference between the three discrete states (a, b and c, shown for a heteronuclear two-spin system) is the orientation of the tensor characterizing the anisotropic interaction (dipolar coupling, CSA and quadrupolar). b) Schematic depiction of the total Liouvillian in the composite space of the three states used in simulations with dynamics. In a first step, the matrix representations of the subsystem Hamiltonians $\hat{H}_{[a]}$, $\hat{H}_{[b]}$ and $\hat{H}_{[c]}$, containing all spin-spin and spin-field interactions relevant for the corresponding state, are computed in Hilbert space. The Liouvillian super operators for each state (e.g. $\hat{\hat{L}}_{[a]}$) can then easily be computed as the commutation super operator of the subsystem Hamiltonians and combined to yield the Liouvillian $\hat{\hat{L}}$ in the composite space. Exchange between the states is included through the addition of the exchange matrix $\hat{\hat{K}}$, shown here for the symmetric three-site exchange process. Depending on the recoupling scheme, the Liouvillian computed from the radio-frequency Hamiltonian also has to be included.

3.1.1 Pulsed Dipolar Recoupling

Measuring order parameters from incompletely averaged dipolar couplings under MAS usually requires the use of a pulse sequence that reintroduces the dipolar interaction. A variety of such recoupling sequences has been developed that are based on different approaches (Nielsen et al., 2012). In this work, we study the apparent recoupling behaviour of three different pulse schemes: (i) Hartmann-Hahn cross polarization (Hartmann and Hahn, 1962; Pines et al., 1972; Stejskal et al., 1977) that was proposed first and is used most often to achieve polarization transfer, (ii) Rotational-Echo Double Resonance (REDOR) (Gullion and Schaefer, 1989; Gullion, 1998) that works best in dilute spin systems under fast MAS and (iii) the more recently developed windowed Phase-Alternating R-symmetry Sequence (wPARS) (Hou et al., 2014; Lu et al., 2016) that can be used in protonated systems at intermediate MAS frequencies since it performs also homonuclear decoupling. Schematic depictions of the corresponding pulse schemes can be found in Fig. 2. In the CP experiment, the dipolar coupling is reintroduced by matching the rf field strengths on the two channels to one of the zero- or double-quantum Hartmann-Hahn matching conditions ($\nu_{1\mathrm{I}} \pm \nu_{1\mathrm{S}} = n\nu_{\mathrm{r}}$). In general, CP is mostly used to transfer polarization from high-γ nuclei such as protons to low-γ nuclei in order to increase the signal-to-noise ratio in spectra of low-γ nuclei. However, heteronuclear dipolar couplings can be determined by incrementing the CP contact time and measuring the full recoupling curve.

In the REDOR scheme, the dipolar coupling is reintroduced by trains of rotor synchronized π pulses. The REDOR curve is then computed as $\Delta S(\tau)/S_0(\tau) = (S_0(\tau) - S(\tau))/S_0(\tau)$, where $S_0(\tau)$ corresponds to the signal measured in a reference

https://doi.org/10.5194/mr-2024-4
Preprint. Discussion started: 21 February 2024

Open Access MAGNETIC RESONANCE Discussions

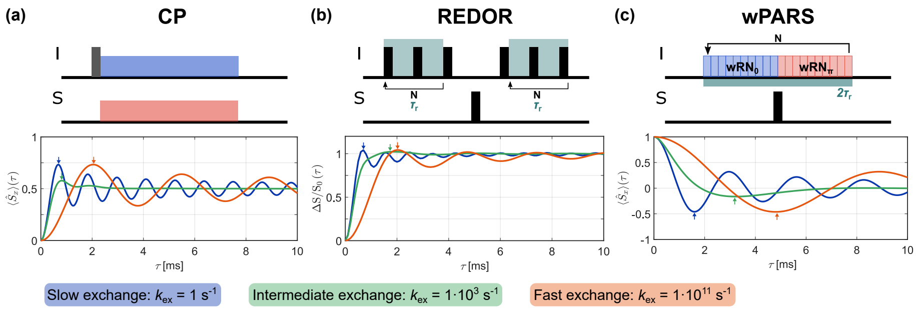

Figure 2. Examples of simulated dipolar recoupling curves for (a) CP, (b) REDOR, and (c) wPARS for slow, intermediate and fast exchange (20 kHz MAS, $\delta_{\mathrm{IS}}/(2\pi) = 5$ kHz, $\theta = 70.5°$). In the intermediate exchange regime, a damping of the oscillations is observed while fast exchange simply leads to a scaling of the dipolar coupling and, thus, a reduction of the oscillation frequency. The apparent δ_{IS} is determined by χ^2-fitting a set of reference simulations with different heteronuclear dipolar couplings without exchange to the initial build-up of the recoupling curve (up to the first local extremum, position indicated by arrows).

experiment without the π pulses on the I spins and $S(\tau)$ is the signal for the REDOR experiment. The normalization of the signal with respect to a reference experiment ensures that the signal decay (due to relaxation) does not need to be accounted for when fitting. The features of the curve, thus, exclusively report on the tensor parameters of the heteronuclear dipolar coupling and the detailed shape of the curve can also unambiguously reveal a non-zero tensor asymmetry that can be fit (Schanda et al., 2011; Asami and Reif, 2019).

The wPARS experiment on the other hand uses a symmetry-based sequence (Zhao et al., 2001; Levitt, 2007) with a basic R element for the recoupling. In this recoupling scheme, a $\mathrm{R}N_0$ block and its π-phase shifted counterpart $\mathrm{R}N_\pi$ are applied on the I channel in an alternating fashion. Each of the $\mathrm{R}N$ blocks contains a standard $\mathrm{R}N_n^\nu$ cycle comprising N basic R elements (π pulses) that are synchronized with n rotor cycles. Pulse phases alternate between ϕ and $-\phi$, where $\phi = \pi\nu/N$ is the phase shift between neighboring pairs of R elements. On the S channel, π pulses are applied between $\mathrm{R}N_0$ and $\mathrm{R}N_\pi$ blocks in order to suppress the CSA of the I spins that would otherwise also be recoupled by the R sequence. In principle, any $\mathrm{R}N_n^\nu$ sequence that recouples the dipolar interaction can be used and we chose to simulate the $\mathrm{R}10_1^3$ sequence due to its reasonable rf requirements for moderate MAS frequencies ($\nu_1 = 5 \cdot \nu_{\mathrm{r}}$).

Examples of simulated recoupling curves for slow ($k_{\mathrm{ex}} = 1$ s^{-1}), intermediate ($k_{\mathrm{ex}} = 1 \cdot 10^3$ s^{-1}) and fast ($k_{\mathrm{ex}} = 1 \cdot 10^{11}$ s^{-1}) exchange at 20 kHz MAS are shown in Fig. 2 for the three pulsed recoupling sequences. Simulations are shown for a dipolar coupling with $\delta_{\mathrm{IS}}/(2\pi) = 5$ kHz and a motional amplitude of $\theta = 70.5°$ (further examples can be found in Figs. S6, S7 and S8 in the SI). The recoupling curves for all three sequences show the characteristic oscillations, that define the frequency which depends on the residual dipolar coupling and, thus, the scaling factor that results for the specific pulse scheme. As expected, the oscillation frequency is reduced for fast exchange due to the scaling of the anisotropic interaction by the rapid molecular motion. In the intermediate exchange regime, strong damping of the oscillation is observed. Additionally, a decay of

https://doi.org/10.5194/mr-2024-4
Preprint. Discussion started: 21 February 2024

MAGNETIC RESONANCE
Open Access
Discussions

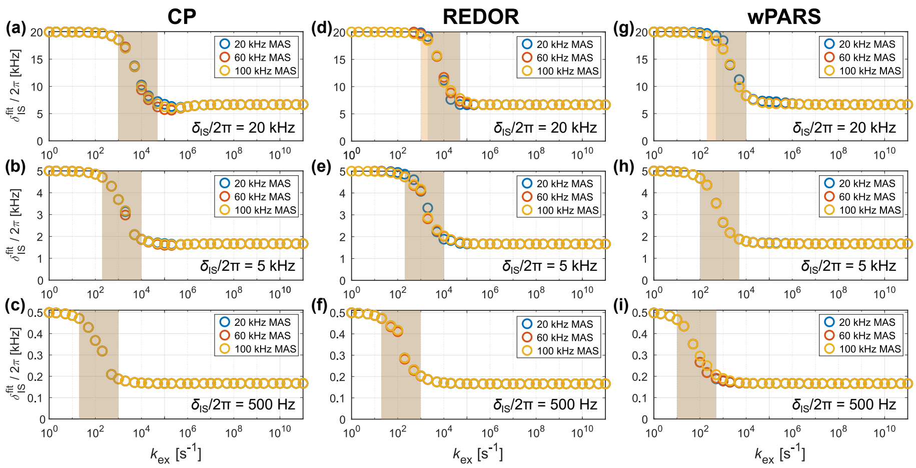

Figure 3. Fitted apparent anisotropy of the dipolar-coupling tensor $\delta_{\mathrm{IS}}^{\mathrm{fit}}$ for CP (a-c), REDOR (d-f) and wPARS (g-i) for different MAS frequencies (20, 60 and 100 kHz) and dipolar-coupling strengths ($\delta_{\mathrm{IS}}/(2\pi)$ = 20, 5 and 0.5 kHz). The underlying molecular motion was modeled using a three-site jump process with an opening angle of $\theta = 70.5°$ (order parameter $S_{\mathrm{IS}} = -1/3$), which corresponds to the case of a sp^3-hybridised carbon site. The rf field strengths used for the recoupling are summarized in Table S2 in the SI. For slow exchange, the full dipolar coupling is retained, while the scaled interaction is observed for fast exchange. In the intermediate exchange regime, a smooth transition from the full to the scaled coupling is observed (shaded area, defined as the region where the difference between two consecutive fitted $\delta_{\mathrm{IS}}^{\mathrm{fit}}$ exceeds 6 % of the difference between the full and scaled δ_{IS} used in the simulations). The position of this transition region depends on the coupling strength and occurs at slower motions for smaller couplings. The MAS frequency only has a marginal effect on the location of the intermediate regime.

magnetization is observed for CP when strong dipolar couplings and longer contact times are considered (see Fig. S1 in the SI).

The apparent $\delta_{\mathrm{IS}}^{\mathrm{fit}}$ can be extracted from the simulated recoupling curves by comparison with a set of reference simulations without exchange. Due to the damping of the oscillations in the intermediate exchange regime (see Fig. 2), only the initial build-up of the curve up to the first local extremum was used for the χ^2-fit. In principle, the observed decay of the recoupling curve in the intermediate regime can be included in the fit by using a two-dimensional grid with an additional line-broadening parameter λ_{lb}. However, no change of the obtained $\delta_{\mathrm{IS}}^{\mathrm{fit}}$ ensued for such a 2D grid (see Fig. S4 in the SI for a comparison of the two fitting routines) and the results presented here stem from fits without λ_{lb}. The resulting $\delta_{\mathrm{IS}}^{\mathrm{fit}}$ as a function of the exchange-rate constant k_{ex} are shown in Fig. 3 for different MAS frequencies and dipolar-coupling strengths. For slow exchange, the full (unscaled) dipolar coupling is observed while fast exchange results in the scaling of the anisotropic interaction by a factor of $1/3$ (as expected for an opening angle of $\theta = 70.5°$). A smooth transition from the full to the scaled interaction is observed in the intermediate exchange regime. The transition region is shaded to facilitate the visual comparison between different sets of simulations and is defined as the region where the difference between two consecutive fitted $\delta_{\mathrm{IS}}^{\mathrm{fit}}$ exceeds 6% of the difference between the full and scaled δ_{IS} used in the simulations. The position of this transition region depends strongly

https://doi.org/10.5194/mr-2024-4
Preprint. Discussion started: 21 February 2024

Open Access MAGNETIC RESONANCE Discussions

on the strength of the interaction. For weaker dipolar couplings, slower motion results in the scaling of the observed coupling and the transition region occurs for smaller values of k_{ex}. The transition region roughly spans motional time scales over two orders of magnitude between 1/10 and 10 times the magnitude of the dipolar coupling. However, the exact position varies depending on the recoupling sequence used. For all three pulse sequences investigated, only a negligible dependence on the MAS frequency is observed. Simulations at 500 kHz MAS (see Fig. S3 in the SI) further suggest that the influence of the MAS frequency will remain unimportant even if significant advances in the achievable spinning frequency are realized in the future. Similar results are obtained for other CP matching conditions (different rf fields at the same MAS frequency, see Fig. S2 in the SI) and REDOR simulations with different π pulse lengths (see Fig. S5 in the SI). The rf field strength, therefore, does not seem to influence the transition from the full to the scaled coupling significantly.

As mentioned above, only the part of the recoupling curve up to the first local extremum (minimum or maximum) was used for the fitting. Since the simulated curves are ideal and noise-free, the initial slope characterizes the magnitude of the effective coupling perfectly. In experimental spectra, it is advisable to fit the observed oscillations in order to get an unambiguous result for the effective coupling strength. However, this will not work in the transition region since the oscillations are overdamped (see Fig. 2) preventing the extraction of effective coupling strength from data with experimental uncertainties. Even in the ideal simulated data, fitting longer mixing times produced strongly varying results for the magnitude of the scaled coupling in the transition region. Therefore, we believe that reliable results from the overdamped curves in the transition region cannot be obtained from experimental data.

In the limit of fast exchange, the order parameter of the dynamic process and, thus, the opening angle θ in our three-site jump model (see Fig. 1a for the bond geometry) determines the scaling of the motion. Figure 4a-c shows a comparison of the fitted apparent $\delta_{\mathrm{IS}}^{\mathrm{fit}}$ for different opening angles for a dipolar coupling of $\delta_{\mathrm{IS}}/(2\pi) = 5$ kHz at a MAS frequency of 20 kHz for CP, REDOR and wPARS. As expected, more restricted motion leads to a larger scaling factor for the incompletely averaged coupling. However, the position and width of the transition region does not seem to be affected significantly.

All three recoupling sequences presented here can be modified to allow the scaling of the effective dipolar coupling. Based on the observed dependence of the position of the transition region on the strength of the anisotropic interaction (see Fig. 3), one could expect that this will enable studying different motional time scales. In the CP experiment, the dipolar coupling strength can be scaled down by tilting one of the two applied spinlock fields away from the transverse plane (van Rossum et al., 2000; Hong et al., 2002). This is schematically depicted in Fig. 4d. The extent of the scaling is characterized by the tilt angle ϑ_1 (where $\vartheta_1 = 90°$ corresponds to the unscaled "normal" CP experiment). Figure 4d shows a comparison of the resulting $\delta_{\mathrm{IS}}^{\mathrm{fit}}$ for $\vartheta_1 = 90°$ and 20° for a dipolar coupling anisotropy of 5 kHz. Examples of recoupling curves for different tilt angles are shown in Fig. S6 in the SI. Changing the tilt angle of the applied rf field on one of the channels does indeed affect the intermediate exchange regime where the transition from the full to the motionally averaged dipolar coupling occurs. The magnitude of the effective dipolar coupling scales with $\cos\vartheta_1$ requiring exceedingly small angles ϑ_1 to achieve a significant scaling. Therefore,

https://doi.org/10.5194/mr-2024-4
Preprint. Discussion started: 21 February 2024

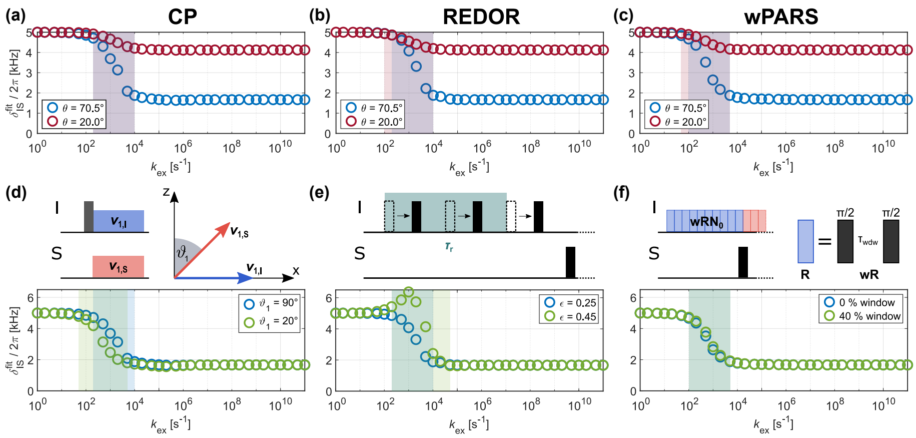

Figure 4. Fitted apparent $\delta_{\mathrm{IS}}^{\mathrm{fit}}$ for CP, REDOR and wPARS for: a-c) different opening angles θ (see Fig. 1a for the geometry of the jump process) and d-f) modifications of the pulse sequence that lead to a scaling of the effective heteronuclear dipolar coupling. Data is shown for a MAS frequency of 20 kHz and $\delta_{\mathrm{IS}}/(2\pi) = 5\,\mathrm{kHz}$. Examples of the corresponding recoupling curves can be found in Figs. S6, S7 and S8 in the SI. In contrast to the amplitude of the motion, the modification of the pulse sequence can affect the transition region (shaded area, defined as the region where the difference between two consecutive fitted $\delta_{\mathrm{IS}}^{\mathrm{fit}}$ exceeds 6 % of the difference between the full and scaled δ_{IS} used in the simulations).

the magnitude of the experimentally achievable shift in the transition region will be limited. We do not expect that significant gain in information on the distribution of motions can be obtained from such angle-dependent measurements due to the inherent low precision of the determined order parameters.

For the REDOR experiment, several schemes exist that allow scaling down the effective dipolar coupling. Strong dipolar couplings result in a rapid build-up of the REDOR curve, which often limits the amount of points on the curve that can be measured experimentally before the signal has decayed. In these cases, REDOR schemes that involve shifting the position of the rotor synchronized π pulses are often used. Here, we study the two-pulse shifted REDOR scheme (Jain et al., 2019a), in which the position of both π pulses within a rotor period is altered while keeping the time separation between them constant at $0.5\tau_{\mathrm{r}}$ (see Fig. 4e). This results in the scaling of the effective dipolar coupling by $\sin(2\pi\epsilon)$, where ϵ characterizes the pulse shift (see Fig. S7 in the SI for further details) and the classic REDOR experiment corresponds to $\epsilon = 0.25$. Apparent $\delta_{\mathrm{IS}}^{\mathrm{fit}}$ for $\epsilon = 0.25$ and 0.45 are shown in Fig. 4e for $\delta_{\mathrm{IS}}/(2\pi) = 5$ kHz. In the limit of fast and slow exchange, the simulated REDOR curves for $\epsilon = 0.45$ and $\delta_{\mathrm{IS}}/(2\pi) = 5$ kHz (corresponding to $\delta_{\mathrm{IS}}^{\mathrm{eff}}/(2\pi) = \sin(2\pi\epsilon)\cdot\delta_{\mathrm{IS}}/(2\pi) = 1545$ Hz) agree well with those obtained for a dipolar coupling with $\delta_{\mathrm{IS}}/(2\pi) = 1545$ Hz in a classic REDOR experiment (see Fig. S7 in the SI). This indicates that shifting the pulse positions in these exchange regimes (ca. $k_{\mathrm{ex}} < 1\cdot 10^2\ \mathrm{s}^{-1}$ and $k_{\mathrm{ex}} > 1\cdot 10^5\ \mathrm{s}^{-1}$ for this particular coupling strength) has the desired scaling effect. However, changing the position of the π pulses strongly affects the appearance of the REDOR curve in the intermediate exchange regime. A shift parameter of $\epsilon \neq 0.25$ leads to a rapid build-up of the REDOR curve and removes the characteristic oscillations. Extracting the apparent $\delta_{\mathrm{IS}}^{\mathrm{fit}}$ for motion on these time scales $(1\cdot 10^2$

https://doi.org/10.5194/mr-2024-4
Preprint. Discussion started: 21 February 2024

$s^{-1} < k_{ex} < 1 \cdot 10^5$ s^{-1} for $\delta_{IS}/(2\pi) = 5$ kHz) is, therefore, impractical and the resulting values contain no real information (see Fig. 4e for fit results). This pulse-shifted implementation of the REDOR experiment thus seems to only be suitable for sufficiently slow or fast dynamics where the full or the motionally averaged interaction is observed. The time scales of these "fast" or "slow" motions depend on the strength of the unscaled dipolar coupling itself (see Fig. 3g-i).

The wPARS sequence allows scaling up the effective dipolar coupling by introducing a window without rf irradiation in the basic R element (see Fig. 4f for a schematic depiction) (Lu et al., 2016). The larger the fraction of time of this window in the basic element, the larger the observed effective coupling. Examples of simulated recoupling curves for different window lengths are shown in Fig. S8 in the SI for a dipolar coupling anisotropy of 5 kHz. Similar to our observations for CP, the effect of the dynamic process on the appearance of the recoupling curves is the same for all window lengths. However, the range of scaling factors that can be achieved is too small to result in a considerable shift of the transition region from the full to the motionally averaged coupling (see Fig. 4f).

In the intermediate exchange regime where the transition from the full to the scaled dipolar coupling occurs, line broadening due to the underlying dynamics and thus overdamped oscillations are observed during the recoupling (see Fig. 2 and Fig. S1 in the SI). This decay of magnetization and the damping of the oscillations in the recoupling curve make the extraction of the tensor parameters difficult even in the noise-free simulated data. In an experimental measurement, other steps in the experiment will also be affected by line broadening. Decay of transverse magnetization (T_2 relaxation) during the detection period for example will broaden spectral lines and reduce resolution. The observed T_2 will depend on a variety of factors, e.g. the coupling strength, the MAS frequency and the decoupling scheme employed (Schanda and Ernst, 2016). A detailed discussion of these effects is beyond the scope of the manuscript. Moreover, dynamics on the intermediate time scale have been shown to have detrimental effects on polarization-transfer experiments (Nowacka et al., 2013; Callon et al., 2022; Aebischer and Ernst, 2024) and will, thus, reduce the signal-to-noise ratio. Extracting reliable information for systems undergoing dynamics on an intermediate time scale from experimental data will, therefore, be impractical in most cases.

3.1.2 Off-Magic-Angle Spinning

Instead of using rf irradiation to reintroduce ansiotropic interactions under MAS, off-magic-angle spinning (off-MAS) can be used to measure order parameters. Changing the tilt of the sample spinning axis with respect to the external B_0 field away from the magic angle reintroduces a scaled anisotropic interaction. The magnitude of the scaled interaction depends on the offset from the magic angle $\theta_{\mathrm{rot}} = \theta_{\mathrm{m}} + \Delta$, where θ_{rot} corresponds to the angle between the external field and the rotation axis and the scaling factor is given by $P_2(\cos\theta_{\mathrm{rot}})$. Experimentally, the reintroduction of the scaled interaction will result in scaled powder patterns and information on any underlying motion can be gained from a line shape analysis. This was first used to study molecular re-orientation by fitting CSA line shapes in one- and two-dimensional ^{13}C CPMAS spectra for different offset angles (Schmidt and Vega, 1989; Blümich and Hagemeyer, 1989) and has also been extended to quadrupolar nuclei

https://doi.org/10.5194/mr-2024-4
Preprint. Discussion started: 21 February 2024

MAGNETIC RESONANCE Discussions
Open Access

(Kustanovich et al., 1991). However, large angle offsets significantly deteriorate spectral resolution. For heteronuclear dipolar couplings, residual couplings can also manifest in perturbations of the J modulation observed in a spin-echo experiment. In this case, small offset angles $|\Delta| < 0.5°$ suffice to introduce significant residual couplings in directly bound spin pairs without notably deteriorating the spectral resolution. Such measurements were first demonstrated for homonuclear dipolar couplings in ^{13}C spin pairs (Pileio et al., 2007) but have since also been used to determine order parameters in backbone amides (Xue et al., 2019b) and methyl groups (Xue et al., 2019a) in deuterated protein samples.

Following the work of Pileio et al. (Pileio et al., 2007), the powder-averaged dephasing signal for a scalar coupled heteronuclear spin pair under off-MAS with small angle offsets is approximately given by

$$S_{\mathrm{mod}}(\tau,\Delta) \approx \frac{1}{2}\int_0^{\pi} \cos\left(\pi J\tau - \sqrt{2}\Delta\frac{\delta_{\mathrm{IS}}}{2}P_2(\cos\beta_{\mathrm{PR}})\tau\right)\sin(\beta_{\mathrm{PR}})\,d\beta_{\mathrm{PR}}\,, \tag{1}$$

where δ_{IS} corresponds to the anisotropy of the dipolar coupling, β_{PR} denotes the angle between the internuclear vector and the rotor axis and P_2 is the second-order Legendre polynomial. The offset of the rotation angle from the magic angle is given by Δ and can be positive or negative. Depending on the relative sign of the scalar J and the dipolar coupling, positive or negative angle offsets can reduce or increase the observed modulation frequency.

Figure 5a-c shows examples of simulated dephasing curves in a heteronuclear spin pair with parameters based on a backbone amide group (NH, $J =$ -90 Hz, $\delta_{\mathrm{IS}}/(2\pi) = 21$ kHz, corresponding to an effective N-H distance of 1.05 Å) for slow ($k_{\mathrm{ex}} = 1\cdot 10^{-2}\ \mathrm{s}^{-1}$), intermediate ($k_{\mathrm{ex}} = 1\cdot 10^{3}\ \mathrm{s}^{-1}$) and fast exchange ($k_{\mathrm{ex}} = 1\cdot 10^{11}\ \mathrm{s}^{-1}$) and different angle offsets. In principle, positive offset angles should increase the observed modulation frequency due to the opposite signs of the dipolar and the J coupling. This is indeed observed in the case of slow exchange. However, the underlying three-site jump process for an opening angle of $\theta = 70.5°$ (see Fig. 1a) results in an order parameter of $-1/3$ and thus a sign change for the apparent δ_{IS}. Smaller opening angles ($\theta < 54.74°$) of the jump model will lead to a positive order parameter and no sign change in the value of the residual dipolar coupling. Positive angle offsets, therefore, reduce the oscillation frequency in the limit of fast exchange for our set of parameters. Larger offset angles result in a more significant distortion of the modulated signal. In the intermediate exchange regime, relaxation results in a decay of magnetization and a damping of the oscillation.

As described in the Methods section, the apparent δ_{IS} was determined by χ^2-fitting a set of reference simulations without exchange (ca. 80 ms observation window). In order to account for the observed signal decay due to relaxation, a two-dimensional grid with the additional line broadening parameter λ_{lb} was used for the fitting. The resulting $\delta_{\mathrm{IS}}^{\mathrm{fit}}$ and the corresponding λ_{lb} are shown in Fig. 5d for different spinning frequencies ($\Delta = 0.05°$) and Fig. 5e for different angle offsets (20 kHz spinning frequency). In the limit of slow ($k_{\mathrm{ex}} < 1\ \mathrm{s}^{-1}$) and fast exchange ($k_{\mathrm{ex}} > 1\cdot 10^{7}\ \mathrm{s}^{-1}$), the full and scaled dipolar coupling are obtained as expected. For intermediate exchange ($k_{\mathrm{ex}} \approx 1\cdot 10^{5}\ \mathrm{s}^{-1}$) the oscillations in the dephasing curves are dampened and no meaningful information on δ_{IS} can be gained (see Fig. S9 in the SI for contour plots of χ^2). The observed line broadening

https://doi.org/10.5194/mr-2024-4
Preprint. Discussion started: 21 February 2024

MAGNETIC RESONANCE Discussions

strongly depends on the spinning frequency and is reduced for faster spinning (see Fig. 5d).

Compared to simulations of pulsed dipolar recoupling under MAS for the same coupling strength (see Fig. 3) the transition from the full to the incompletely averaged interaction occurs for significantly slower motion. This can be attributed to the scaling of the dipolar coupling by the small angle offset (see Eq. (1)) and the position of the transition can be shifted by changing the angle offset (see Fig. 5e). The scaling of the dipolar coupling by off-MAS does not affect the motional time scales for which rapid relaxation is observed. Therefore, the range of exchange-rate constants where the transition towards the scaled interaction occurs is separated from the regions where the signal decays fast. This separation is further improved for even faster spinning frequencies (see Fig. S10 in the SI for simulation results at 500 kHz spinning), suggesting off-MAS as a suitable method for characterizing dynamics at fast MAS. This is in contrast to the rf irradiation based recoupling under MAS described above, where the transition region always coincides with the region of rapid relaxation.

For exchange-rate constants around $1 \cdot 10^2\ \mathrm{s}^{-1}$, the sign of the anisotropy of the dipolar coupling is not well defined (see Fig. S9 in the SI for more details), leading to jumps in the resulting $\delta_{\mathrm{IS}}^{\mathrm{fit}}$ (see Fig. 5d and e). In this exchange regime, the dipolar coupling is scaled to values close to zero since the underlying three-site jump leads to a sign change of δ_{IS} for faster motion. The jumps in the fitted $\delta_{\mathrm{IS}}^{\mathrm{fit}}$ can thus be attributed to the sign change of the dipolar coupling for faster motion. For a lower amplitude of motion (see Fig. 5f for simulation results for an opening angle of $\theta = 20.0^\circ$ corresponding to an order parameter of $S_{\mathrm{IS}} \approx 0.82$) no such jumps in the fitted $\delta_{\mathrm{IS}}^{\mathrm{fit}}$ are observed. In this case, only the line broadening in the intermediate exchange regime deteriorates the fit quality.

3.2 CSA Recoupling

The chemical-shift anisotropy, like the dipolar coupling, is averaged by molecular motion. To investigate how motion on different time scales influences this averaging, we performed CSA simulations using a symmetry-based sequence ($\mathrm{R}18_1^7$); this class of $\mathrm{R}N_n^\nu$ sequences are among the most popular techniques for CSA recoupling (Levitt, 2007; Hou et al., 2012). The sequences consists of a train of π pulses with alternating phases $\pm\phi = \pm\pi\nu/N = \pm 70^\circ \cdot (\pi/180^\circ)$, applied to the nucleus of which the CSA is to be recoupled. The rf-field strength is chosen such that N (here: $N = 18$) π pulses fit into n (here: $n = 1$) rotor periods; in the case of $\mathrm{R}18_1^7$, the nutation frequency of the rf field is, thus, nine times the MAS frequency. The CSA parameters can be obtained from the evolution of the signal amplitude as a function of the duration of the recoupling sequence, by either fitting the time-domain or the frequency-domain signal. Here, we fitted the apparent CSA tensor anisotropy, $\delta_{\mathrm{CSA}}^{\mathrm{fit}}$, in the time domain with a χ^2 minimization procedure, comparing the simulations with dynamics against a grid of simulated rigid-limit recoupling trajectories. As for the dipolar recoupling, only the initial build-up of the curves was fitted.

Figure 6a shows examples of CSA recoupling trajectories for slow ($k_{\mathrm{ex}} = 1\ \mathrm{s}^{-1}$), intermediate ($k_{\mathrm{ex}} = 1 \cdot 10^3\ \mathrm{s}^{-1}$) and fast exchange ($k_{\mathrm{ex}} = 1 \cdot 10^{11}\ \mathrm{s}^{-1}$). As for the dipolar recoupling (see Fig. 2), the frequency of the modulation is high, and identical to

https://doi.org/10.5194/mr-2024-4
Preprint. Discussion started: 21 February 2024

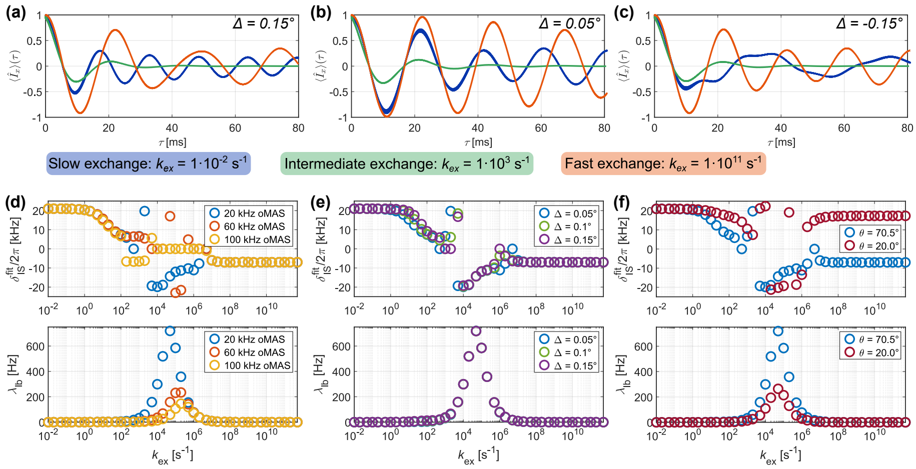

Figure 5. Simulated off-magic angle spinning of a heteronuclear NH two-spin system with a scalar coupling of $J =$ -90 Hz and a dipolar coupling of $\delta_{\mathrm{IS}}/(2\pi) = 21$ kHz. a-c) Examples of simulated dephasing of proton transverse magnetization $\hat{I}_x$ for spinning at different offset angles Δ (20 kHz spinning frequency, $\theta = 70.5°$). d-f) Fitted $\delta_{\mathrm{IS}}^{\mathrm{fit}}$ and line broadening parameter λ_{lb} as a function of the exchange-rate constant for off-angle spinning simulations: d) $\Delta = 0.05°$ and different spinning frequnecies, e) 20 kHz spinning and different angle offsets, f) $\Delta = 0.05°$ and 20 kHz spinning for different motional amplitudes (see Fig. 1a for the underlying exchange process).

the rigid case, for slow exchange, and scaled down for very fast exchange. In the intermediate regime, the recoupling trajectory shows strong dampening and decays to zero. The fitted apparent $\delta_{\mathrm{CSA}}^{\mathrm{fit}}$ is plotted against the time scale of the underlying motion in Fig. 6b-d for different CSA strengths of $\delta_{\mathrm{CSA}}/(2\pi) = 20$, 5 and 0.5 kHz, respectively. The transition from the slow regime, where the CSA is not averaged, to the fast regime is found to depend on the rigid-limit tensor anisotropy. The larger the rigid-limit CSA anisotropy, the shorter the time scale at which the transition from the fast regime to the slow regime occurs. For example, the mid-point of the transition occurs at an exchange-rate constant of $k_{\mathrm{ex}} = 5 \cdot 10^3\ \mathrm{s}^{-1}$ if the rigid-limit CSA anisotropy is 20 kHz, whereas the transition is found at approximately $k_{\mathrm{ex}} = 1 \cdot 10^2\ \mathrm{s}^{-1}$ if the anisotropy is 0.5 kHz. The opening angle θ of the underlying jump model (see Fig. 1a) also changes the scaling of the CSA at fast time scales (Fig. 2e) but has no significant effect on the width and position of the transition region. Overall, the CSA recoupling shows similar trends as the dipolar recoupling in terms of the time scales over which it reports averaging.

3.3 Quadrupoles

In addition to dipolar couplings and CSA tensors, incompletely averaged quadrupolar couplings can be used to study dynamics in solid-state NMR (Shi and Rienstra, 2016; Akbey, 2022, 2023). Under MAS, the first-order quadrupolar coupling becomes time-dependent and results in spinning sideband patterns while the second-order quadrupolar coupling leads to line broadening and isotropic shifts. The intensity distribution of these sideband spectra can be used to determine the anisotropy of the quadrupolar coupling and, thus, reveals information on the time scale and amplitude of the motional process. In biological systems, deuterium (^{2}H) is often used in such studies, where it is introduced either uniformly or selectively to replace a specific

https://doi.org/10.5194/mr-2024-4
Preprint. Discussion started: 21 February 2024

MAGNETIC RESONANCE
Open Access
Discussions

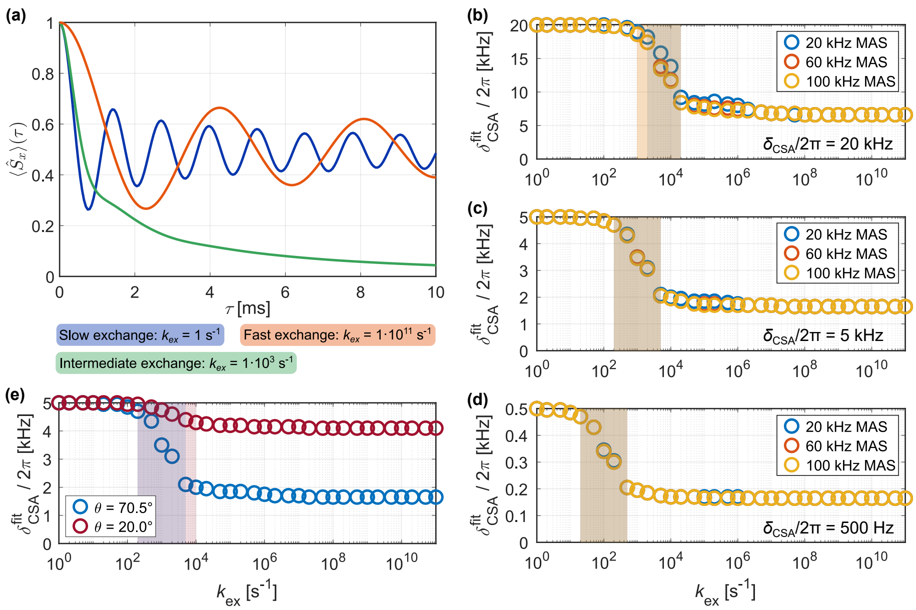

Figure 6. Apparent recoupling behaviour for $R18_1^7$ recoupling of the CSA interaction in the presence of molecular motion. a) Examples of recoupling curves for slow, intermediate and fast exchange (20 kHz MAS, $\delta_{\mathrm{CSA}}/(2\pi) = 5$ kHz, $\theta = 70.5°$). For fast exchange, a lower frequency oscillation corresponding to the scaled CSA interaction is observed. Motion on an intermediate time scale results in a strong damping of the oscillations and signal decay. b-d) MAS dependence of fit results for different interaction strengths. e) Comparison of fitted apparent $\delta_{\mathrm{CSA}}^{\mathrm{fit}}$ for different opening angles θ (20 kHz MAS, $\delta_{\mathrm{CSA}}/(2\pi) = 5$ kHz).

^{1}H nucleus. Deuterium has a spin-1 with a quadrupolar coupling constant C_{qcc} of approximately 160 kHz. Although used less often than dipolar couplings or CSA tensors, the ^{2}H line shapes in static samples or the spinning sideband pattern under MAS are commonly analyzed to probe protein dynamics (Hologne et al., 2006; Shi and Rienstra, 2016; Akbey, 2023; Vugmeyster and Ostrovsky, 2017).

Figure 7 shows examples of simulated side-band manifolds for deuterium (assuming $\delta_{\mathrm{Q}}/(2\pi) = 80$ kHz or C_{qcc} = 160 kHz) undergoing a symmetric three-site exchange process at 20 kHz MAS. The quadrupolar tensors of the three sites were assumed to be axially symmetric and aligned with the bond geometry depicted in Fig. 1a. As expected, fast exchange results in the scaling of the quadrupolar coupling and, thus, a narrower side-band spectrum is observed. The extent of the scaling is again dependent on the opening angle of the three-site jump process and more restricted motion leads to a scaling factor closer to one. In the intermediate exchange regime (roughly $1 \cdot 10^3\ \mathrm{s}^{-1} < k_{\mathrm{ex}} < 1 \cdot 10^7\ \mathrm{s}^{-1}$) strong line broadening is observed. As described in the Methods Section, apparent $\delta_{\mathrm{Q}}^{\mathrm{fit}}$ were obtained by χ^2 fitting a two-dimensional grid of reference simulations without exchange and an additional line broadening parameter λ_{lb}. An observation window of approximately 150 ms corresponding to a signal intensity of less than 1 % for a spectral line with 10 Hz full width at half maximum was used in the fitting procedure. Prior to χ^2 fitting, a frequency shift (implemented as a first-order phase correction in time domain) was applied in time-domain

https://doi.org/10.5194/mr-2024-4
Preprint. Discussion started: 21 February 2024

MAGNETIC RESONANCE
Open Access
Discussions

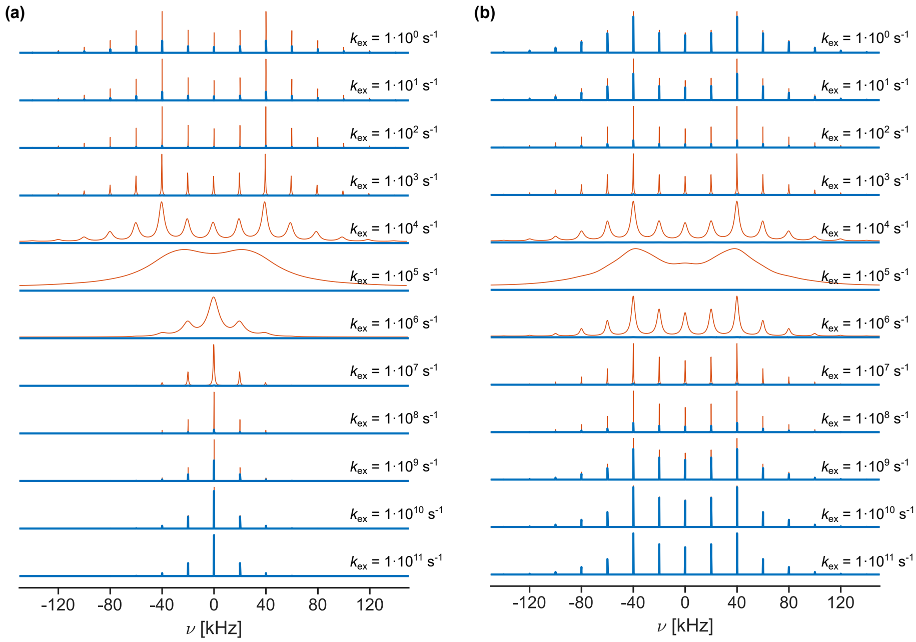

Figure 7. Simulated spectra of ^{2}H with $\delta_{\mathrm{Q}}/(2\pi) = 80\,\mathrm{kHz}$ at 20 kHz MAS for different exchange-rate constants for opening angles of $\theta = 70.5°$ (a) and 20° (b) (see Fig. 1a for the geometry of the exchange process). The intensity of spectra shown as thick blue lines was normalized to the maximum intensity observed for all exchange-rate constants while spectra shown as thin red lines were normalized to their respective maximum intensity. All spectra were processed with 10 Hz exponential line broadening. For exchange-rate constants around $1 \cdot 10^{5}\ \mathrm{s}^{-1}$, the sideband manifold is broadened beyond detection due to rapid relaxation.

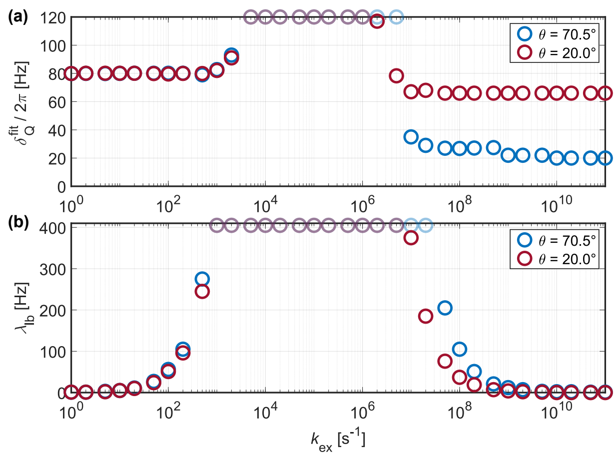

Figure 8. Fitted $\delta_{\mathrm{Q}}^{\mathrm{fit}}$ (a) and line broadening parameter λ_{lb} (b) for simulations of ^{2}H with $\delta_{\mathrm{Q}}/(2\pi) = 80$ kHz at 20 kHz MAS for different opening angles of the three-site jump model (see Fig. 1a for the geometry of the exchange process). In the intermediate-exchange regime, the observed line broadening exceeds the reference grid of δ_{Q} and λ_{lb} used for the χ^{2}-fit, resulting in a plateau of fitted values (data points shown with reduced opacity).

https://doi.org/10.5194/mr-2024-4
Preprint. Discussion started: 21 February 2024

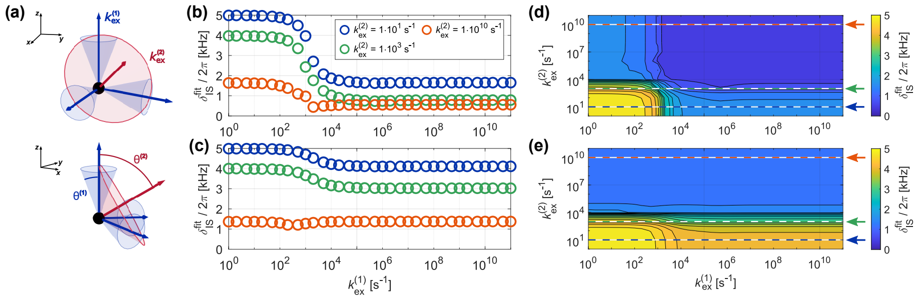

Figure 9. a) Schematic representation of the exchange process used to model more complex motion as a simultaneous inner and outer motion. The inner motion is described by a three-site jump process modeling rotation about the inner C_3-axis (blue arrows, rotation on blue cones with an opening angle of $\theta^{(1)}$), while the outer motion rotates the subsets of three sites each about the outer C_3-axis (red arrow, rotation on red cone with an opening angle of $\theta^{(2)}$). b-e) Apparent recoupling behaviour for a dipolar coupled heteronuclear two-spin system ($\delta_{\mathrm{IS}}/(2\pi) = 5$ kHz) for CP recoupling at 20 kHz MAS ($\nu_{1\mathrm{I}} = 93$ kHz, $\nu_{1\mathrm{S}} = 73$ kHz). b-c) Fitted $\delta_{\mathrm{IS}}^{\mathrm{fit}}$ as a function of $k_{\mathrm{ex}}^{(1)}$ for different $k_{\mathrm{ex}}^{(2)}$ for $\theta^{(1)} = \theta^{(2)} = 70.5°$ (b) and $\theta^{(1)} = 20.0°$ and $\theta^{(2)} = 70.5°$ (c). d-e) Contour plots of $\delta_{\mathrm{IS}}^{\mathrm{fit}}$ as a function of both $k_{\mathrm{ex}}^{(1)}$ and $k_{\mathrm{ex}}^{(2)}$ for $\theta^{(1)} = \theta^{(2)} = 70.5°$ (d) and $\theta^{(1)} = 20.0°$ and $\theta^{(2)} = 70.5°$ (e). The position of the one-dimensional slices shown in b and c are indicated by dashed lines.

to ensure that the central peak in the sideband manifold has a frequency offset of zero. Fit results are shown in Fig. 8 for two different opening angles of the jump process. Compared to the dipolar and CSA interaction, significantly faster motion ($k_{\mathrm{ex}} > 1 \cdot 10^8$ s^{-1}) is required to average the quadrupolar coupling due to its large magnitude. Moreover, the transition region from the full to the motionally averaged interaction is broader than for the CSA and the dipolar coupling. In the intermediate exchange regime, strong line broadening leads to featureless spectra and the true λ_{lb} of the simulated FIDs exceeds the values considered in the grid for the fit. This makes the extraction of information for molecular motion on these time scales practically impossible. In the limit of fast exchange, the quality of the χ^2 fit deteriorates (see Fig. S11 in the SI) due to slight differences in the frequency offset of the central peak in the sideband manifold. Nevertheless, the expected scaling depending on the order parameter of the dynamic process is observed. This suggests that the measurement of the quadrupolar coupling can only give insight in the limit of fast or sufficiently slow motion.

3.4 Multiple Motions

Molecular motion is usually more complex than a simple rotation about an axis and often several motions on different time scales occur simultaneously. In order to study potential effects in such systems, we extended the three-site exchange model to a nine-site jump process that encompasses two independent rotations about non-collinear C_3-axes (see Fig. 9a). The inner motion is modeled by a three-site jump process with an amplitude described by $\theta^{(1)}$ within subsets of three sites. The jump process describing the outer motion leads to exchange between sites within the different subsets. Its amplitude is defined by the tilt angle between the inner C_3-axes and its own symmetry axis ($\theta^{(2)}$). As an example, the apparent recoupling behaviour

https://doi.org/10.5194/mr-2024-4
Preprint. Discussion started: 21 February 2024

Open Access MAGNETIC RESONANCE Discussions

for CP recoupling for different time scales of the inner and outer motion is shown in Fig. 9b-e. The fitted apparent $\delta_{\mathrm{IS}}^{\mathrm{fit}}$ for $\theta^{(1)} = \theta^{(2)} = 70.5°$ is shown in Figs. 9b and d, while Figs. 9c and e shows simulation results for an inner motion with a smaller amplitude ($\theta^{(1)} = 20.0°$ and $\theta^{(2)} = 70.5°$). When both motions are slow ($k_{\mathrm{ex}} < 1 \cdot 10^2\ \mathrm{s}^{-1}$ for the $\delta_{\mathrm{IS}}/(2\pi) = 5$ kHz considered here), the full interaction is observed. When both motions are fast on the other hand (ca. $k_{\mathrm{ex}} > 1 \cdot 10^5\ \mathrm{s}^{-1}$), the scaled interaction is observed, where the total scaling factor corresponds to $P_2(\cos\theta^{(1)}) \cdot P_2(\cos\theta^{(2)})$. If the amplitude of the inner motion is small and the motion is sufficiently fast, the transition region for the outer motion is shifted (see Fig. 9e), since the inner motion already leads to a scaling of the dipolar coupling. The effects for motion on intermediate time scales depends on the amplitude of the two motions and the relative speed of the inner and outer motion and are difficult to predict in general.

4 Conclusions

We have investigated the averaging of anisotropic interactions in solid-state NMR under MAS using numerical simulations based on the stochastic Liouville equation. Simple jump models with a three-fold symmetry and equal populations were used to simplify the characterization of the partially averaged couplings using a single order parameter. In all cases, the time scale of the dynamics defines three distinct regions: slow motion where the full anisotropic interaction is retained, fast motion where a scaled anisotropic interaction is obtained and an intermediate region where a transition from the full to the scaled anisotropic interaction is observed. The time scales included in the three regions depend on the magnitude of the interaction and, to a much lower extent, on the method used to measure the anisotropic quantity while the MAS frequency has a negligible influence.

Heteronuclear one-bond H-X dipolar couplings are the most often measured interactions for the characterization of the amplitude of motion (order parameter), and are often combined with relaxation studies. The position of the transition region depends on the magnitude of the dipolar coupling. For typical heteronuclear one-bond (e.g., NH, CH) dipolar couplings with an anisotropy of $\delta_{\mathrm{IS}}/(2\pi)$ on the order of several 10 kHz, the transition region starts at $k_{\mathrm{ex}} \approx 10^3$ s^{-1} and ends roughly at 10^5 s^{-1} with minor differences between different recoupling methods. Smaller dipolar couplings shift the transition region to slower time scales. A scaling of the effective dipolar couplings by pulsed recoupling methods only has a minor influence on the position of the transition area but can influence the spectra obtained in the transition region strongly.

The determination of dipolar couplings using off-magic angle spinning behaves differently from the other methods: the transition region starts at much slower rate constants (around 1 s^{-1}) and extends to roughly 1 s^3. However, for MAS frequencies up to 100 kHz the end of the transition region overlaps with the motional time scales for which efficient transverse relaxation is observed. Thus, the range of exchange-rate constants for which the anisotropy of the dipolar coupling is difficult to determine is extended to rate constants up to 10^7 s^{-1}. Only for off-magic angle spinning, the transition region does not coincide with motional time scales that cause rapid transverse relaxation. The extended dynamic time scales towards slower motions covered by off-magic angle spinning is mirrored by the large range of dynamics down to millisecond time scales obtained in residual

https://doi.org/10.5194/mr-2024-4
Preprint. Discussion started: 21 February 2024

dipolar couplings in partially aligned liquids (Blackledge, 2005).

The measurement of scaled CSA tensors behaves similarly to the dipolar couplings since it is based on the same principles. For a CSA tensor with an anisotropy of $\delta_{\mathrm{CSA}}/(2\pi)$ = 5 kHz, the transition area starts at about $k_{\mathrm{ex}} \approx 10^2$ s^{-1} and ends roughly at 10^4 s^{-1} and is independent of the MAS frequency.

Quadrupolar couplings (typically ^{2}H or ^{14}N) under MAS do not require active recoupling due to their typically larger magnitude. They can be measured directly using the side-band pattern of the first-order quadrupolar coupling. Again a transition region is observed between rate constants $k_{\mathrm{ex}} \approx 10^3$ s^{-1} and 10^7 s^{-1} where strong line broadening makes the determination of the side-band pattern impossible. For exchange-rate constants larger than 10^7 s^{-1}, scaled quadrupolar couplings are obtained while the full coupling is measured for exchange-rate constants smaller than 10^3 s^{-1}.

In our simulations, the transition region shows a smooth transition from the full unscaled anisotropic interaction to the scaled one in many cases. In principle, one could determine the time scale of motion from the measured dipolar coupling in this region. However, in practice this is not likely to provide useful results. Firstly, one does not know the full motional amplitude in the fast-exchange limit in general; thus, it is not always possible to interpret an observed value in the transition region. Moreover, and of great practical relevance, motion on a time scale that corresponds to the transition region of dipolar/CSA/quadrupolar averaging generally strongly deteriorates spectral quality since motion on this μs time scale induces strong transverse relaxation. This leads to an overdamping of the oscillations, making the quantification of the coupling in realistic noisy experimental data hopeless. Therefore, no quantitative information is available in the intermediate region in practical cases. Off-magic angle spinning experiments are an exception, however, because the time scales where the transition of the dipolar averaging occurs is separated from the time scale where strongest relaxation occurs. In off-magic angle experiments, relaxation is still determined by the full anisotropic interaction and fast relaxation is observed for rate constants in the $k_{\mathrm{ex}} \approx 10^3$ s^{-1} to 10^5 s^{-1} range, as in experiments with spinning at the magic angle. The transition from full to scaled interaction, however, is shifted to slower motions due to the reduced magnitude of the rotationally averaged anisotropic interactions.

Combining measurements of large anisotropic interactions (e.g., quadrupolar couplings) with measurements of intermediate (e.g., one-bond-heteronuclear dipolar couplings or CSA tensors) and small anisotropic interactions (e.g., off-magic angle spinning) might be a possibility to characterize the amplitude of motion in different time windows. However, care has to be taken that all interactions probe the same set of motions. While such a combination of different experiments that are sensitive to anisotropic interactions could be a way to gain information on the time scales of motion, relaxation-based experiments appear to be the better and more robust and reliable way of accessing time scales of dynamics.

Code and data availability. The data will be made available through the ETH library data services after potential revisions.

Author contributions. ME and PS designed the research, KA and LB carried out the simulations and data analysis. KA wrote the first draft of the manuscript with support from LB. All authors discussed the results and were involved in finalizing the manuscript.

Competing interests. At least one of the (co-)authors is a member of the editorial board of Magnetic Resonance. The authors have no other competing interests to declare.

Acknowledgements. L. M. B. is recipient of a DOC fellowship of the Austrian Academy of Sciences at the Institute of Science and Technology Austria (DOC-OEAW, PR10660EAW01). This research has been supported by the ETH Zürich and the Schweizerischer Nationalfonds zur Förderung der Wissenschaftlichen Forschung (grant nos. 200020_188988 and 200020_219375).

https://doi.org/10.5194/mr-2024-4
Preprint. Discussion started: 21 February 2024

References

Abergel, D. and Palmer, A. G.: On the use of the stochastic Liouville equation in nuclear magnetic resonance: Application to $R_{1\rho}$ relaxation in the presence of exchange, Concepts Magn. Reson. A, 19A, 134–148, https://doi.org/10.1002/cmr.a.10091, 2003.

Aebischer, K. and Ernst, M.: INEPT and CP transfer efficiencies of dynamic systems in MAS solid-state NMR, J. Magn. Reson., 359, 107 617, https://doi.org/10.1016/j.jmr.2024.107617, 2024.

Akbey, Ü.: Site-specific protein methyl deuterium quadrupolar patterns by proton-detected 3D ^{2}H–^{13}C–^{1}H MAS NMR spectroscopy, J. Biomol. NMR, 76, 23–28, https://doi.org/10.1007/s10858-021-00388-4, 2022.

Akbey, Ü.: Site-specific protein backbone deuterium $^{2}H^{\alpha}$ quadrupolar patterns by proton-detected quadruple-resonance 3D $^{2}H^{\alpha}C^{\alpha}$NH MAS NMR spectroscopy, Solid State Nucl. Magn. Reson., 125, 101 861, https://doi.org/10.1016/j.ssnmr.2023.101861, 2023.

Asami, S. and Reif, B.: Accessing Methyl Groups in Proteins via ^{1}H-detected MAS Solid-state NMR Spectroscopy Employing Random Protonation, Scientific Reports, 9, 15 903, https://doi.org/10.1038/s41598-019-52383-3, 2019.

Blackledge, M.: Recent progress in the study of biomolecular structure and dynamics in solution from residual dipolar couplings, Progress in Nuclear Magnetic Resonance Spectroscopy, 46, 23 – 61, https://doi.org/10.1016/j.pnmrs.2004.11.002, 2005.

Blümich, B. and Hagemeyer, A.: Two-dimensional ^{13}C exchange spectroscopy with off-magic angle spinning, Chem. Phys. Lett., 161, 55–59, https://doi.org/10.1016/S0009-2614(89)87031-9, 1989.

Brüschweiler, R.: Dipolar averaging in NMR spectroscopy: From polarization transfer to cross relaxation, Progress in Nuclear Magnetic Resonance Spectroscopy, 32, 1 – 19, http://links.isiglobalnet2.com/gateway/Gateway.cgi?GWVersion=2&SrcAuth=mekentosj&SrcApp=Papers&DestLinkType=FullRecord&DestApp=WOS&KeyUT=000072552700001, 1998.

Callon, M., Malär, A. A., Lecoq, L., Dujardin, M., Fogeron, M., Wang, S., Schledorn, M., Bauer, T., Nassal, M., Böckmann, A., and Meier, B. H.: Fast Magic-Angle-Spinning NMR Reveals the Evasive Hepatitis B Virus Capsid C-Terminal Domain, Angew. Chem., 134, e202201 083, https://doi.org/10.1002/ange.202201083, 2022.

Cheng, V. B., Suzukawa, H. H., and Wolfsberg, M.: Investigations of a nonrandom numerical method for multidimensional integration, J. Chem. Phys., 59, 3992–3999, https://doi.org/10.1063/1.1680590, 1973.

Chevelkov, V., Fink, U., and Reif, B.: Accurate Determination of Order Parameters from ^{1}H , ^{15}N Dipolar Couplings in MAS Solid-State NMR Experiments, J. Am. Chem. Soc., 131, 14 018–14 022, https://doi.org/10.1021/ja902649u, 2009.

Chevelkov, V., Lange, S., Sawczyc, H., and Lange, A.: Accurate Determination of Motional Amplitudes in Biomolecules by Solid-State NMR, ACS Phys. Chem. Au, 3, 199–206, https://doi.org/10.1021/acsphyschemau.2c00053, 2023.

Concistrè, M., Carignani, E., Borsacchi, S., Johannessen, O. G., Mennucci, B., Yang, Y., Geppi, M., and Levitt, M. H.: Freezing of Molecular Motions Probed by Cryogenic Magic Angle Spinning NMR, J. Phys. Chem. Lett., 5, 512–516, https://doi.org/10.1021/jz4026276, pMID: 26276602, 2014.

Gauto, D. F., Macek, P., Barducci, A., Fraga, H., Hessel, A., Terauchi, T., Gajan, D., Miyanoiri, Y., Boisbouvier, J., Lichtenecker, R., Kainosho, M., and Schanda, P.: Aromatic Ring Dynamics, Thermal Activation, and Transient Conformations of a 468 kDa Enzyme by Specific ^{1}H–^{13}C Labeling and Fast Magic-Angle Spinning NMR, J. Am. Chem. Soc., 141, 11 183–11 195, https://doi.org/10.1021/jacs.9b04219, 2019.

Gullion, T.: Introduction to rotational-echo, double-resonance NMR, Concepts in Magnetic Resonance, 10, 277–289, https://doi.org/10.1002/(SICI)1099-0534(1998)10:5<277::AID-CMR1>3.0.CO;2-U, 1998.

https://doi.org/10.5194/mr-2024-4
Preprint. Discussion started: 21 February 2024

Gullion, T. and Schaefer, J.: Rotational-echo double-resonance NMR, J. Magn. Reson., 81, 196 – 200, https://doi.org/10.1016/0022-2364(89)90280-1, 1989.

Haller, J. D. and Schanda, P.: Amplitudes and time scales of picosecond-to-microsecond motion in proteins studied by solid-state NMR: a critical evaluation of experimental approaches and application to crystalline ubiquitin, J. Biomol. NMR, 57, 263–280, https://doi.org/10.1007/s10858-013-9787-x, 2013.

Harris, C. R., Millman, K. J., der Walt, S. J., Gommers, R., Virtanen, P., Cournapeau, D., Wieser, E., Taylor, J., Berg, S., Smith, N. J., Kern, R., Picus, M., Hoyer, S., van Kerkwijk, M. H., Brett, M., Haldane, A., del Río, J. F., Wiebe, M., Peterson, P., Gérard-Marchant, P., Sheppard, K., Reddy, T., Weckesser, W., Abbasi, H., Gohlke, C., and Oliphant, T. E.: Array programming with NumPy, Nature, 585, 357–362, https://doi.org/10.1038/s41586-020-2649-2, 2020.

Hartmann, S. R. and Hahn, E. L.: Nuclear double resonance in the rotating frame, Phys. Rev., 128, 2042, https://doi.org/10.1103/PhysRev.128.2042, 1962.

Hologne, M., Chen, Z., and Reif, B.: Characterization of dynamic processes using deuterium in uniformly ^{2}H, ^{13}C, ^{15}N enriched peptides by MAS solid-state NMR, J. Magn. Reson., 179, 20–28, https://doi.org/10.1016/j.jmr.2005.10.014, 2006.

Hong, M.: Structure, Topology, and Dynamics of Membrane Peptides and Proteins from Solid-State NMR Spectroscopy, J. Phys. Chem. B, 111, 10 340–10 351, https://doi.org/10.1021/jp073652j, 2007.

Hong, M., Yao, X., Jakes, K., and Huster, D.: Investigation of Molecular Motions by Lee-Goldburg Cross-Polarization NMR Spectroscopy, J. Phys. Chem. B, 106, 7355–7364, https://doi.org/10.1021/jp0156064, 2002.

Hou, G., Byeon, I.-J. L., Ahn, J., Gronenborn, A. M., and Polenova, T.: ^{1}H–^{13}C/^{1}H–^{15}N Heteronuclear Dipolar Recoupling by R-Symmetry Sequences Under Fast Magic Angle Spinning for Dynamics Analysis of Biological and Organic Solids, J. Am. Chem. Soc., 133, 18 646–18 655, https://doi.org/10.1021/ja203771a, 2011.

Hou, G., Byeon, I.-J. L., Ahn, J., Gronenborn, A. M., and Polenova, T.: Recoupling of chemical shift anisotropy by R-symmetry sequences in magic angle spinning NMR spectroscopy., J. Chem. Phys., 137, 134 201, https://doi.org/10.1063/1.4754149, 2012.

Hou, G., Lu, X., Vega, A. J., and Polenova, T.: Accurate measurement of heteronuclear dipolar couplings by phase-alternating R-symmetry (PARS) sequences in magic angle spinning NMR spectroscopy, J. Chem. Phys., 141, https://doi.org/10.1063/1.4894226, 2014.

Hunter, J. D.: Matplotlib: A 2D graphics environment, Computing in Science & Engineering, 9, 90–95, https://doi.org/10.1109/MCSE.2007.55, 2007.

Jain, M. G., Mote, K. R., Hellwagner, J., Rajalakshmi, G., Ernst, M., Madhu, P. K., and Agarwal, V.: Measuring strong one-bond dipolar couplings using REDOR in magic-angle spinning solid-state NMR, J. Chem. Phys., 150, 134 201, https://doi.org/10.1063/1.5088100, 2019a.

Jain, M. G., Rajalakshmi, G., Agarwal, V., Madhu, P., and Mote, K. R.: On the direct relation between REDOR and DIPSHIFT experiments in solid-state NMR, J. Magn. Reson., 308, 106 563, https://doi.org/10.1016/j.jmr.2019.07.050, 2019b.

Krushelnitsky, A., Reichert, D., and Saalwächter, K.: Solid-state NMR approaches to internal dynamics of proteins: From picoseconds to microseconds and seconds, Acc. Chem. Res., 46, 2028–2036, https://doi.org/10.1021/ar300292p, 2013.

Kubo, R.: Stochastic Liouville Equations, J. Math. Phys., 4, 174–183, https://doi.org/10.1063/1.1703941, 1963.

Kustanovich, I., Vega, S., and Zaborowski, E.: Dynamic off-magic-angle sample spinning NMR of deuterium, J. Magn. Reson. (1969), 93, 441–446, https://doi.org/10.1016/0022-2364(91)90023-M, 1991.

Lamley, J. M. and Lewandowski, J. R.: Relaxation-based magic-angle spinning NMR approaches for studying protein dynamics, eMagRes, 5, 1423–1434, https://doi.org/10.1002/9780470034590.emrstm1417, 2016.

Lamley, J. M., Lougher, M. J., Sass, H.-J., Rogowski, M., Grzesiek, S., and Lewandowski, J. R.: Unraveling the complexity of protein backbone dynamics with combined ^{13}C and ^{15}N solid-state NMR relaxation measurements, Phys. Chem. Chem. Phys., 17, 21 997–22 008, https://doi.org/10.1039/C5CP03484A, 2015.

Levitt, M. H.: Symmetry-Based Pulse Sequences in Magic-Angle Spinning Solid-State NMR, John Wiley & Sons, Ltd, ISBN 9780470034590, https://doi.org/10.1002/9780470034590.emrstm0551, 2007.

Lewandowski, J. R.: Advances in Solid-State Relaxation Methodology for Probing Site-Specific Protein Dynamics, Acc. Chem. Res., 46, 2018–2027, https://doi.org/10.1021/ar300334g, 2013.

Lorieau, J. L. and McDermott, A. E.: Conformational Flexibility of a Microcrystalline Globular Protein: Order Parameters by Solid-State NMR Spectroscopy, J. Am. Chem. Soc., 128, 11 505–11 512, https://doi.org/10.1021/ja062443u, 2006.

Lu, X., Zhang, H., Lu, M., Vega, A. J., Hou, G., and Polenova, T.: Improving dipolar recoupling for site-specific structural and dynamics studies in biosolids NMR: windowed RN-symmetry sequences, Phys. Chem. Chem. Phys., 18, 4035–4044, https://doi.org/10.1039/C5CP07818K, 2016.

Martin, R. W., Kelly, J. E., and Collier, K. A.: Spatial reorientation experiments for NMR of solids and partially oriented liquids, Prog. Nucl. Magn. Reson. Spectrosc., 90, 92–122, https://doi.org/10.1016/j.pnmrs.2015.10.001, 2015.

Moro, G. J. and Freed, J. H.: Efficient computation of magnetic resonance spectra and related correlation functions from stochastic Liouville equations, J. Phys. Chem., 84, 2837 – 2840, https://doi.org/10.1021/j100459a001, 1980.

Munowitz, M. G., Griffin, R. G., Bodenhausen, G., and Huang, T. H.: Two-dimensional rotational spin-echo nuclear magnetic resonance in solids: correlation of chemical shift and dipolar interactions, J. Am. Chem. Soc., 103, 2529–2533, https://doi.org/10.1021/ja00400a007, 1981.

Nielsen, N. C., Strassø, L. A., and Nielsen, A. B.: Dipolar recoupling., Topics in Current Chemistry, 306, 1 – 45, https://doi.org/10.1007/128_2011_129, 2012.

Nowacka, A., Bongartz, N., Ollila, O., Nylander, T., and Topgaard, D.: Signal intensities in ^{1}H–^{13}C CP and INEPT MAS NMR of liquid crystals, J. Magn. Reson., 230, 165–175, https://doi.org/10.1016/j.jmr.2013.02.016, 2013.

Pileio, G., Guo, Y., Pham, T. N., Griffin, J. M., Levitt, M. H., and Brown, S. P.: Residual Dipolar Couplings by Off-Magic-Angle Spinning in Solid-State Nuclear Magnetic Resonance Spectroscopy, J. Am. Chem. Soc., 129, 10 972–10 973, https://doi.org/10.1021/ja0721115, 2007.

Pines, A., Gibby, M. G., and Waugh, J. S.: Proton-Enhanced Nuclear Induction Spectroscopy. A Method for High Resolution NMR of Dilute Spins in Solids, J. Chem. Phys., 56, 1776–1777, https://doi.org/10.1063/1.1677439, 1972.

Schanda, P. and Ernst, M.: Studying dynamics by magic-angle spinning solid-state NMR spectroscopy: Principles and applications to biomolecules, Prog. Nucl. Magn. Reson. Spectr., 96, 1–46, https://doi.org/10.1016/j.pnmrs.2016.02.001, 2016.

Schanda, P., Meier, B. H., and Ernst, M.: Quantitative Analysis of Protein Backbone Dynamics in Microcrystalline Ubiquitin by Solid-State NMR Spectroscopy, J. Am. Chem. Soc., 132, 15 957–15 967, https://doi.org/10.1021/ja100726a, 2010.

Schanda, P., Huber, M., Boisbouvier, J., Meier, B. H., and Ernst, M.: Solid-State NMR Measurements of Asymmetric Dipolar Couplings Provide Insight into Protein Side-Chain Motion, Angew. Chem. Int. Ed., 50, 11 005–11 009, https://doi.org/10.1002/anie.201103944, 2011.

Schmidt, A. and Vega, S.: Dynamic off-magic-angle sample spinning NMR spectroscopy, Chem. Phys. Lett., 157, 539–542, https://doi.org/10.1016/S0009-2614(89)87407-X, 1989.

Shi, X. and Rienstra, C. M.: Site-Specific Internal Motions in GB1 Protein Microcrystals Revealed by 3D ^{2}H– ^{13}C–^{13}C Solid-State NMR Spectroscopy, J. Am. Chem. Soc., 138, 4105–4119, https://doi.org/10.1021/jacs.5b12974, 2016.

https://doi.org/10.5194/mr-2024-4
Preprint. Discussion started: 21 February 2024

MAGNETIC RESONANCE Discussions
Open Access

Smith, A. A., Ernst, M., and Meier, B. H.: Optimized "detectors" for dynamics analysis in solid-state NMR, J. Chem. Phys., 148, 045 104, https://doi.org/10.1063/1.5013316, 2018.

Smith, S. A., Levante, T. O., Meier, B. H., and Ernst, R. R.: Computer simulations in magnetic resonance. An object-oriented programming approach, J. Magn. Reson., 106, 75–105, https://doi.org/10.1006/jmra.1994.1008, 1994.

Stejskal, E. O., Schaefer, J., and Waugh, J. S.: Magic-angle spinning and polarization transfer in proton-enhanced NMR, J. Magn. Reson., 28, 105–112, https://doi.org/10.1016/0022-2364(77)90260-8, 1977.

van Rossum, B.-J., de Groot, C. P., Ladizhansky, V., Vega, S., and de Groot, H. J. M.: A Method for Measuring Heteronuclear (^{1}H-^{13}C) Distances in High Speed MAS NMR, J. Am. Chem. Soc., 122, 3465–3472, https://doi.org/10.1021/ja992714j, 2000.

Vega, A. J. and Fiat, D.: Relaxation theory and the stochastic Liouville equation, J. Magn. Reson. (1969), 19, 21–30, https://doi.org/10.1016/0022-2364(75)90024-4, 1975.

Vugmeyster, L. and Ostrovsky, D.: Static solid-state ^{2}H NMR methods in studies of protein side-chain dynamics, Prog. Nucl. Magn. Reson. Spectrosc., 101, 1–17, https://doi.org/10.1016/j.pnmrs.2017.02.001, 2017.

Watt, E. D. and Rienstra, C. M.: Recent advances in solid-state nuclear magnetic resonance techniques to quantify biomolecular dynamics, Anal. Chem., 86, 58–64, https://doi.org/10.1021/ac403956k, 2014.

Xue, K., Mamone, S., Koch, B., Sarkar, R., and Reif, B.: Determination of methyl order parameters using solid state NMR under off magic angle spinning, J. Biomol. NMR, 73, 471–475, https://doi.org/10.1007/s10858-019-00253-5, 2019a.

Xue, K., Mühlbauer, M., Mamone, S., Sarkar, R., and Reif, B.: Accurate Determination of ^{1}H-^{15}N Dipolar Couplings Using Inaccurate Settings of the Magic Angle in Solid-State NMR Spectroscopy, Angew. Chem. Int. Ed., 58, 4286–4290, https://doi.org/10.1002/anie.201814314, 2019b.

Yan, S., Suiter, C. L., Hou, G., Zhang, H., and Polenova, T.: Probing structure and dynamics of protein assemblies by magic angle spinning NMR spectroscopy., Acc. Chem. Res., 46, 2047–58, https://doi.org/10.1021/ar300309s, 2013.

Zhao, X., Eden, M., and Levitt, M. H.: Recoupling of heteronuclear dipolar interactions in solid-state NMR using symmetry-based pulse sequences, Chem. Phys. Lett., 342, 353–361, https://doi.org/10.1016/S0009-2614(01)00593-0, 2001.

Zumpfe, K. and Smith, A. A.: Model-Free or Not?, Front. Mol. Biosci., 8, https://doi.org/10.3389/fmolb.2021.727553, 2021.